THE JOURNAL OF PHYSICAL CHEMISTRY C

Article

pubs.acs.org/JPCC

Variation of the Core Atomic Structure of Thiolated $(Au_xAg_{1-x})_{312\pm55}$ Nanoclusters with Composition from Aberration-Corrected HAADF STEM

Nan Jian and Richard E. Palmer*

Nanoscale Physics Research Laboratory, School of Physics and Astronomy, University of Birmingham, Birmingham, United Kingdom

Supporting Information

ABSTRACT: We have investigated the atomic structure of thiol-protected $(Au_xAg_{1-x})_{312\pm55}$ clusters as a function of composition (x) by using aberration-corrected Scanning Transmission Electron Microscopy (STEM), in High Angle Annular Dark Field (HAADF) mode, combined with multislice electron scattering simulations of the STEM images. Three structural motifs are considered: icosahedral, fcc, and ino-decahedral. A combination of STEM intensity and diameter measurement is used to "fractionate" the deposited sample according to composition for atomic resolution imaging. We find that the structure depends critically on composition: the icosahedral structure dominates in Ag-rich clusters, while the fcc structure dominates in Au-rich clusters. The ino-decahedral structure was only observed in clusters with Au content greater than 30%.

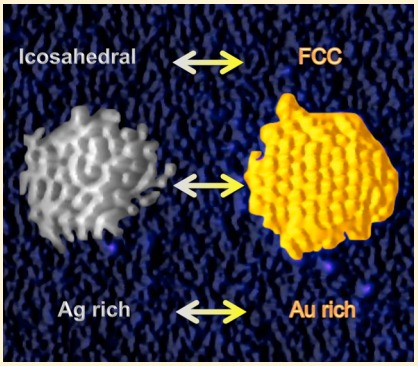

INTRODUCTION

Nanoclusters are extensively studied because of their unique physical, chemical and catalytic properties.[1−5] Small, alloy nanoclusters are of increasing interest[6−11] due to their distinctive size and compositional effects,[6,12] which suggest a number of applications in catalysis, optics, engineering, and electronics. In recent years, research on the synthesis of alloy nanoclusters has demonstrated impressive size and composition control, from sub-10 nm AuAg alloy nanoparticles to size-selected $Au_{25-n}Ag_n(SR)_{18}$, $Au_{38-n}Ag_n(SR)_{24}$, $Au_{144-n}Ag_n(SR)_{60}$, and so on.[13−20] Cu−Au and Pd−Au analogs of the 25-atom and 144-atom species are also reported.[21−24] Such monolayer-protected alloy nanoparticles are a special focus of research.[25−28] Thus, the atomic structures of alloy nanoclusters need to be investigated in order to correlate properties with structure. The lowest energy structures of alloy nanoclusters (up to 50 metal atoms) have been found to be highly affected by material, size, and composition.[29] X-ray crystal structures of $Au_{25-n}Ag_n(SR)_{18}$ and $Au_{44-n}Ag_n(SR)_{30}$ have been determined,[17,30] but the structures of larger alloy clusters are yet to be determined. Research into the lowest energy structures of Ag−Pd nanoclusters with different sizes and compositions shows a strong dependence of structure on composition.[31]

Here we present the atomic structure of phenylethanethiolate-protected (-SCH_2CH_2Ph) Au_xAg_{1-x} bimetallic nanoclusters containing 312 ± 55 atoms, with size and composition determined from STEM. Samples of variable composition are imaged using aberration-corrected STEM and compared with multislice simulation atlases. The projected area of cluster in the STEM images is utilized to determine the total metal nuclearity while calibrated HAADF-STEM integrated intensity measurement was employed to obtain the bimetallic cluster composition. Our results show that the atomic structures of MP-$(Au_xAg_{1-x})_{312\pm55}$ nanoclusters are completely dependent on the composition: most Au-rich cluster structures are fcc, while most Ag-rich clusters are icosahedral. The ino-decahedral structure was only found in clusters with more than 30% Au. The result should be relevant to the catalytic application of this new class of nanosystems.[32−37]

EXPERIMENTAL METHODS

The clusters investigated were provided by the group of Prof. Dass at the University of Mississippi. The method of synthesis is similar to ref 38 and described in the Supporting Information (SI). The product was characterized by Matrix-Assisted Laser Desorption Ionization (MALDI) mass spectrometry (see Figure S3) and shows a mean mass of 59 kDa for all composition clusters produced. The monometallic, Au-only product of the same synthesis was assigned a composition of $Au_{329}(SCH_2CH_2Ph)_{84}$ based on a peak at 76.3 kDa.[38,39] The 1:1 molar ratio of the $HAuCl_4/AgNO_3$ starting materials used in this work yielded a peak at 59 (±4%) kDa, which is quite broad and does not lead to a unique nuclearity and ligand number assignment per se. (We will see below that the STEM data are able to demonstrate the range of core size and metal composition in the nanoparticle distribution after deposition.)

Special Issue: Current Trends in Clusters and Nanoparticles Conference

Received: November 29, 2014
Revised: March 12, 2015
Published: March 13, 2015

DOI: 10.1021/jp5119103
J. Phys. Chem. C 2015, 119, 11114−11119

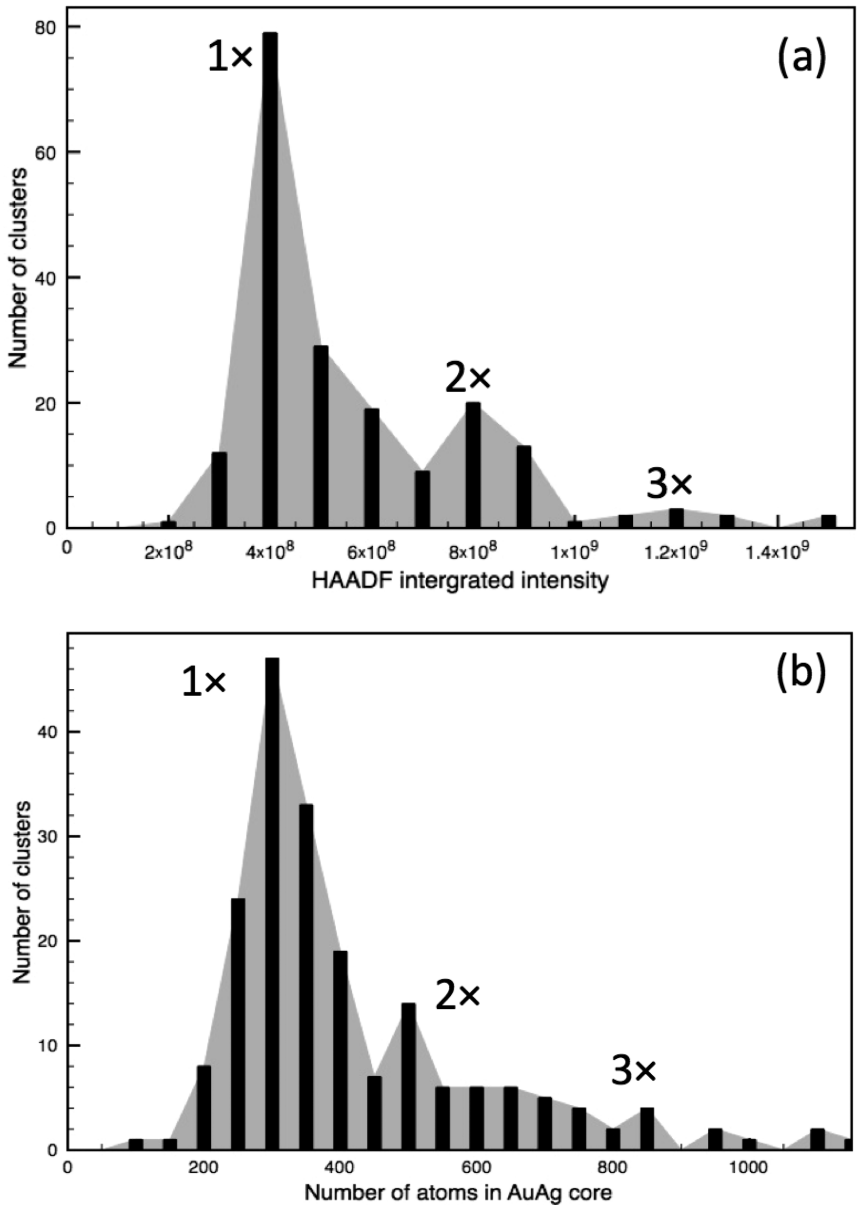

Figure 1. Histogram of (a) HAADF integrated intensity and (b) Au−Ag core nuclearity (obtained from the measured diameters) for 202 individual thiolate protected $(Au_xAg_{1-x})_{312\pm55}$ clusters. Both (a) and (b) show the distributions consistent with discrete multiples of monomers.

However, if we assume that the ligand number is the same as assigned previously to the monometallic species[39] and that the average Au/Ag ratio is 1:1, we obtain from the 59 kDa peak a nuclearity of 312 and thus estimated mean composition of $Au_{156}Ag_{156}(SR)_{84}$.

The dried alloy cluster powder from the final synthetic product was dissolved in toluene and drop cast onto half of a 400-mesh TEM grid covered with an amorphous carbon film. Size-selected Au_{923} clusters (with an error of 5%), which can be easily recognized from alloy clusters, generated with a magnetron sputtering, gas condensation cluster beam source and mass selected with a lateral time-of-flight (TOF) mass selector,[40−42] were deposited onto the other half of the same TEM grid as a calibration tool. The cluster beam current was 50 pA, deposition time 60 s, and the number of clusters deposited was $\sim 1.9 \times 10^{10}$. Our 200 kV JEOL JEM-2100F STEM with Cs corrector (CEOS) was equipped with an HAADF detector operating with an inner angle of 62 mrad and an outer angle of 164 mrad. All images were typically taken in less than 2.7 s (equal to two scans over the whole image area) with an electron dose of $\sim 7.1 \times 10^3$ electrons $Å^{-2}$ at 12 M magnification to minimize beam damage. A 15 min beam shower, without enhanced electron beam at 400 K magnification (total electron dose $\sim 3.4 \times 10^4$ electrons $Å^{-2}$) was employed to minimize the contamination. The beam shower did not damage the sample: images taken before and after beam shower are presented in SI; the results show no evidence of cluster movement or atom loss. The multislice simulations employed corresponded to bare magic-number Au_{309} clusters: cuboctahedral, icosahedral, and ino-decahedral structures were treated with the QSTEM simulation package[43] for comparison with the experimental results.

RESULTS AND DISCUSSION

Before we can investigate the thiolated $(Au_xAg_{1-x})_{312\pm55}$ nanoclusters' atomic structures, the size (i.e., nuclearity) and

DOI: 10.1021/jp5119103
J. Phys. Chem. C 2015, 119, 11114−11119

composition of individual clusters, as found on the surface, are required. The HAADF intensity distribution integrated is shown in Figure 1a. There are three peaks in the distribution, forming a harmonic series, the first peak around 4×10^8 is assigned to be the peak of monomer, while multiples are assigned to dimer and trimer produced by aggregation in solution or on the surface. Since the sample is an alloy, the atom counting method, based simply on the HAADF intensities, as employed for monometallic clusters,[44−46] cannot be applied. Thus, since most clusters observed are approximately circular in projection, we approximate the clusters to spheres and convert the measured area in the STEM images into a volume. Given the bond lengths of Au and Ag are very similar (288.4 pm and 288.9 pm), we can calculate easily the total number of metal atoms in the cluster. The validity of this method is demonstrated against size-selected Au_{561} and Au_{923} clusters, as detailed in the SI.

The number of atoms in each alloy cluster obtained by the method described above is shown in Figure 1b. With this size (nuclearity) information, we can now obtain the composition of each alloy cluster from the atom counting method,[44−46] using size-selected Au clusters as the mass balance. The Au proportion is

$$P_{AU} = \frac{N_{AU}}{N_T} = \frac{k}{k-1} - \frac{I_T - I_{ligand}}{I_{Au\ atom}(k-1) \times N_T}$$
$$k = \left(\frac{Z_{Ag}}{Z_{AU}}\right)^n \quad (1)$$

Here, N_T is the total number of atoms in one Au−Ag alloy cluster, N_{Au} is the number of Au atoms, Z_{Ag} and Z_{Au} are the atomic numbers for Ag and Au, I_T is the total HAADF integrated intensity of cluster, I_{Au} is the intensity of one Au atom (obtained from the size-selected Au_{923} clusters), and I_{ligand} is the intensity of a ligand, based on the calibrated Z-contrast exponent, n ($n = 1.46 \pm 0.18$).[47,48] (In the size region of 312 ± 55, we use a tentative ligand number 84, as previously assigned to the monometallic composition,[39] which is consistent with the MALDI data as noted above.)

After obtaining the nuclearity and composition of the deposited alloy clusters, we can investigate the atomic structure of the $(Au_xAg_{1-x})_{312\pm55}SR_{84}$ clusters with a multislice simulation atlas[49−52] as a function of compositions (x). First, in the high-resolution HAADF-STEM images, all the bimetallic clusters showed intermixing, that is, alloy formation, and no significant core−shell, multishell, or subcluster features were found. Figure 2 shows an illustrative set of high resolution HAADF-STEM images of the Au−Ag alloy clusters with their corresponding simulated images (for bare Au_{309} clusters). Thus, for example, Figure 2(a)−(c) are the experimental images of clusters assigned to fcc structures and (d)−(f) are their corresponding simulated images. These show a good match with the experimental images. Images corresponding to ino-decahedral structures are shown in Figure 2(g)−(i). Icosahedral structure images are shown in Figure 2(m)−(r). Some experimental images did not match the simulated images perfectly. We note that the models used for our simulations are ideal, symmetric, full shell structures, but many clusters grew asymmetrically.[53] For example, in Figure 2(i), the central axis of decahedron is markedly off center. Moreover, we know that the thiol ligands will have a strong effect on the surface of the clusters, with surface Au atom incorporated into the ligand shell.[54,55] These

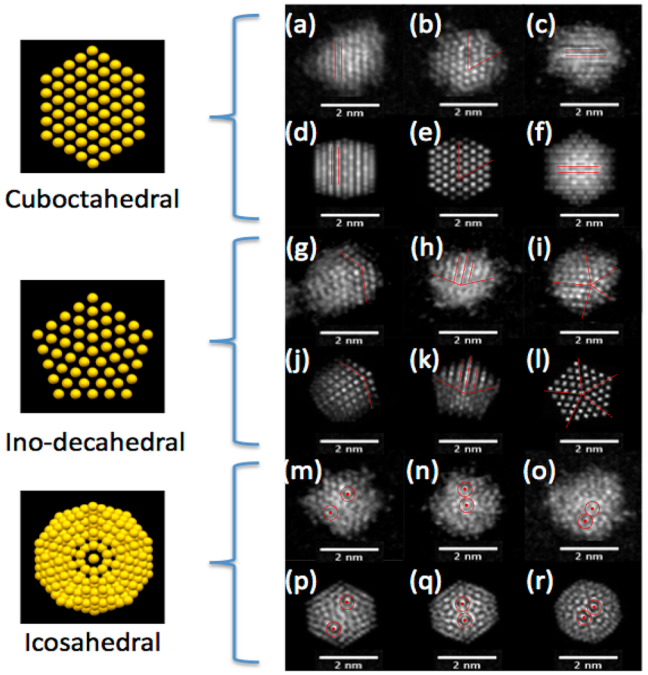

Figure 2. Typical HAADF STEM images of thiolated $(Au_xAg_{1-x})_{312\pm55}$ clusters. (a)−(c), (g)−(i), and (m)−(o) are clusters assigned to cuboctahedral, ino-decahedral, or icosahedral structures, based on (d)−(f), (j)−(l), and (p)−(r), the corresponding simulated images (for bare Au_{309} clusters, which is the closest full shell size of cuboctahedral, icosahedral, and ino-decahedral).

displaced surface atoms will affect the match between the experimental STEM images and the corresponding simulated images. However, the core structure of the clusters can still be recognized,[49,56] via distinctive motifs like the icosahedron's "circle with dot inside" or the 5-fold symmetry of the decahedron, as shown in given specific panels.

Figure 3 shows the main outcome of the work, the relative proportion of different structural isomers of $(Au_xAg_{1-x})_{312\pm55}SR_{84}$ as a function of the Au/Ag compositions. The amorphous or unidentified structure clusters (~42% of all clusters) were removed from the statistics to focus on relative abundance of ordered structures with varying Au/Ag composition. From Figure 3, the Au/Ag composition has a profound impact on the proportion of the different isomers. There is a clear trend, namely, that in the Ag rich region the icosahedral structure is dominant, with the percentage declining smoothly as the Au proportion increases, while the fcc motif, which shows very low abundance in the Ag rich clusters, rises continuously as the Au proportion increases. Their cross over is at a composition of around 40% Au. The decahedron was only found in clusters with a Au content greater than 30%, after which the percentage of decahedral clusters remain between 18 and 30% into the Au-rich region. A comparison analysis of structure distribution of clusters with size of above and below 312 atoms has also been employed to avoid the possibility of size effect on the cluster atomic structures, the result shows no significant difference and remain the trend of the variation of the atomic structure. We note also that the wide range of Ag−Au composition ratio, and indeed the relatively broad range of size, derived from STEM are not reflected in the MALDI mass spectrum (Figure S3) discussed above. Further work is warranted to explore this discrepancy in terms of the fundamental nature of the measurements.

DOI: 10.1021/jp5119103
J. Phys. Chem. C 2015, 119, 11114−11119

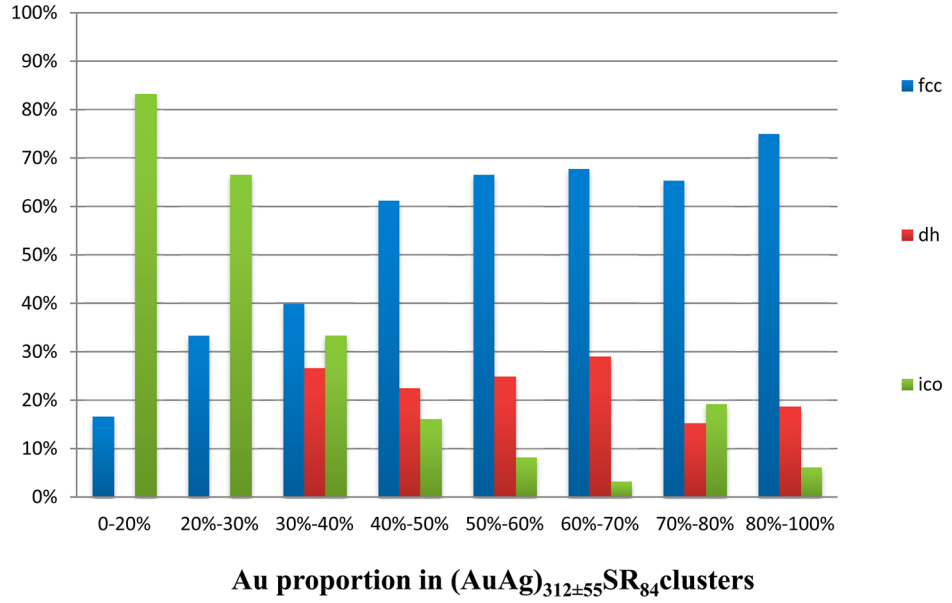

Figure 3. Proportion of the fcc, ino-decahedral, and icosahedral motifs for thiolated $(Au_xAg_{1-x})_{312\pm55}$ clusters with the composition varying from pure Ag (left) to pure Au (right).

Theoretical predictions of the atomic structure of noble metal clusters as a function of size appear to vary widely.[57−59] The experimental results reported here are consistent with theoretical simulations which employed the Gupta potential for clusters. Specifically, this theoretical work finds a transition from icosahedral to fcc structures with increasing size For Au clusters, the crossover size is around 30 atoms, while for Ag the crossover size is much higher, around 300−400 atoms.[57,58] This difference in behavior is associated with the relative values of bulk modulus and cohesive energy in Au and Ag. If we assume that the properties of Au−Ag alloy clusters vary monotonically from Au-rich to Ag-rich clusters, as previous research suggests,[15,60] the theory is entirely compatible with our data for size 312 ± 55 atoms, showing high fcc and low icosahedral proportions in the Au-rich cluster, the opposite for the Ag-rich clusters.

CONCLUSIONS

In conclusion, we have exploited the capability of HAADF-STEM to determine the size of AuAg nanoalloy cluster from the projected areas and the Au−Ag composition from the HAADF intensities calibrated against size-selected clusters. The experimental atomic structures of thiolated $(Au_xAg_{1-x})_{312\pm55}$ clusters deposited on amorphous carbon were compared with multislice image simulation for fcc, icosahedral and decahedral motifs. We found that in the size range of 312 ± 55 atoms, the isomer proportions vary smoothly with the change in composition from pure Ag to Au. The icosahedral structure dominates for Ag-rich composition and fcc dominates the Au-rich region, with the decahedron observed for Au-rich clusters. The work demonstrates the power of aberration-corrected STEM in revealing the atomic structure of bimetallic clusters as a function of composition. The data helps to distinguish between different theoretical approaches and may form a useful test case for future theoretical work. We believe that the experimental approach employed has much potential to be widely to investigate the size, composition, and atomic structures of other binary nanostructures.

ASSOCIATED CONTENT

Supporting Information

Synthesis process of 59 kDa, $(Au_xAg_{1-x})_{312\pm55}$ clusters and additional supporting figures. This material is available free of charge via the Internet at http://pubs.acs.org.

AUTHOR INFORMATION

Corresponding Author

*E-mail: r.e.palmer@bham.ac.uk.

Notes

The authors declare no competing financial interest.

ACKNOWLEDGMENTS

We are grateful to Dr Amala Dass and Chanaka Kumara of the University of Mississippi for kindly providing the alloy cluster samples and for many discussions. We acknowledge financial support from the EPSRC and TSB. The STEM instrument employed in this research was obtained through the Birmingham Science City project "Creating and Characterizing Next Generation Advanced Materials," supported by Advantage West Midlands (AWM) and in part funded by the European Regional Development Fund (ERDF).

REFERENCES

(1) Baletto, F.; Ferrando, R. Structural Properties of Nanoclusters: Energetic, Thermodynamic, and Kinetic Effects. *Rev. Mod. Phys.* **2005**, *77*, 371−423.

(2) de. Heer, W. A. The Physics of Simple Metal Clusters: Experimental Aspects and Simple Models. *Rev. Mod. Phys.* **1993**, *65*, 611−676.

(3) Schmid, G.; Bäumle, M.; Geerkens, M.; Helm, I.; Osemann, C.; Sawitowski, T. Current and Future Applications of Nanoclusters. *Chem. Soc. Rev.* **1999**, *28*, 179−185.

(4) Daniel, M.; Astruc, D. Gold Nanoparticles: Assembly, Supramolecular Chemistry, Quantum-Size-Related Properties, and Applications toward Biology, Catalysis, and Nanotechnology. *Chem. Rev.* **2004**, *104*, 293−346.

(5) Marks, L. Experimental Studies of Small Particle Structures. *Rep. Prog. Phys.* **1994**, *57*, 603−649.

DOI: 10.1021/jp5119103
J. Phys. Chem. C 2015, 119, 11114−11119

(6) Ferrando, R.; Jellinek, J.; Johnston, R. Nanoalloys: From Theory to Applications of Alloy Clusters and Nanoparticles. *Chem. Rev.* **2008**, *108*, 845−910.
(7) Schmid, G.; West, H.; Malm, J. Catalytic Properties of Layered Gold−Palladium Colloids. *Chem.—Eur. J.* **1996**, *2*, 1099−1103.
(8) Caps, V.; Arrii, S.; Morfin, F.; Bergeret, G.; Rousset, J.-L. Structures and Associated Catalytic Properties of Well-Defined Nanoparticles Produced by Laser Vaporisation of Alloy Rods. *Faraday Discuss.* **2008**, *138*, 241−256.
(9) Ferrer, D.; Torres-Castro, A. Three-Layer Core/Shell Structure in Au−Pd Bimetallic Nanoparticles. *Nano Lett.* **2007**, *7*, 1701−1705.
(10) Toshima, N.; Yonezawa, T. Bimetallic Nanoparticles: Novel Materials for Chemical and Physical Applications. *New J. Chem.* **1998**, *22*, 1179−1201.
(11) Yasuda, H.; Kameoka, T.; Sato, T.; Kijima, N.; Yoshimura, Y. Sulfur-Tolerant Pd−Pt/Al_2O_3−B_2O_3 Catalyst for Aromatic Hydrogenation. *Appl. Catal.* **1999**, *185*, 199−201.
(12) Ruban, A.; Skriver, H.; Nørskov, J. Surface Segregation Energies in Transition-Metal Alloys. *Phys. Rev. B* **1999**, *59*, 990−1000.
(13) Li, Y.; Wang, Z. W.; Chiu, C.-Y.; Ruan, L.; Yang, W.; Yang, Y.; Palmer, R. E.; Huang, Y. Synthesis of Bimetallic Pt−Pd Core-Shell Nanocrystals and Their High Electrocatalytic Activity Modulated by Pd Shell Thickness. *Nanoscale* **2012**, *4*, 845−851.
(14) Mallin, M.; Murphy, C. Solution-Phase Synthesis of Sub-10 Nm Au−Ag Alloy Nanoparticles. *Nano Lett.* **2002**, *2*, 10−12.
(15) Kariuki, N.; Luo, J.; Maye, M.; Hassan, S.; Menard, T.; Naslund, H.; Lin, Y.; Wang, C.; Engelhard, M.; Zhong, C. Composition-Controlled Synthesis of Bimetallic Gold−Silver Nanoparticles. *Langmuir* **2004**, *20*, 11240−11246.
(16) Li, Z. Y.; Wilcoxon, J. P.; Yin, F.; Chen, Y.; Palmer, R. E.; Johnston, R. L. Structures and Optical Properties of 4−5 Nm Bimetallic AgAu Nanoparticles. *Faraday Discuss.* **2008**, *138*, 363−373.
(17) Kumara, C.; Aikens, C. M.; Dass, A. X-ray Crystal Structure and Theoretical Analysis of $Au_{25-x}Ag_x(SCH_2CH_2Ph)_{18}$: Alloy. *J. Phys. Chem. C* **2014**, *5*, 461−466.
(18) Kumara, C.; Dass, A. AuAg Alloy Nanomolecules with 38 Metal Atoms. *Nanoscale* **2012**, *4*, 4084−4086.
(19) Jupally, V. R.; Dass, A. Synthesis of $Au_{130}(SR)_{50}$ and $Au(130-x)Ag(x)(SR)_{50}$ Nanomolecules through Core Size Conversion of Larger Metal Clusters. *Phys. Chem. Chem. Phys.* **2014**, *16*, 10473−10479.
(20) Kumara, C.; Dass, A. $(AuAg)_{144}(SR)_{60}$ Alloy Nanomolecules. *Nanoscale* **2011**, *3*, 3064−3067.
(21) Negishi, Y.; Munakata, K.; Ohgake, W.; Nobusada, K. Effect of Copper Doping on Electronic Structure, Geometric Structure, and Stability of Thiolate-Protected Au_{25} Nanoclusters. *J. Phys. Chem. Lett.* **2012**, *25*, 2209−2214.
(22) Negishi, Y.; Kurashige, W.; Niihori, Y.; Iwasa, T.; Nobusada, K. Isolation, Structure, and Stability of a Dodecanethiolate-Protected Pd(1)Au(24) Cluster. *Phys. Chem. Chem. Phys.* **2010**, *12*, 6219−6225.
(23) Dharmaratne, A. C.; Dass, A. $Au(144-x)Cu(x)(SC_6H_{13})_{60}$ Nanomolecules: Effect of Cu Incorporation on Composition and Plasmon-Like Peak Emergence in Optical Spectra. *Chem. Commun. (Cambridge, U.K.)* **2014**, *50*, 1722−1724.
(24) Kothalawala, N.; Kumara, C.; Ferrando, R.; Dass, A. $Au(144-x)Pd(x)(SR)_{60}$ Nanomolecules. *Chem. Commun. (Cambridge, U.K.)* **2013**, *49*, 10850−10852.
(25) Hostetler, M.; Zhong, C.; Yen, B. K. H.; Anderegg, J.; Gross, S. M.; D, E. N.; Porter, M.; Murray. Stable, Monolayer-Protected Metal Alloy Clusters. *J. Am. Chem. Soc.* **1998**, *7863*, 9396−9397.
(26) Philip, R.; Kumar, G. R.; Sandhyarani, N.; Pradeep, T. Picosecond Optical Nonlinearity in Monolayer-Protected Gold, Silver, and Gold−Silver Alloy Nanoclusters. *Phys. Rev. B: Condens. Matter Mater. Phys.* **2000**, *62*, 13160−13166.
(27) Shon, Y. S.; Dawson, G. B.; Porter, M.; Murray, R. W. Monolayer-Protected Bimetal Cluster Synthesis by Core Metal Galvanic Exchange Reaction. *Langmuir* **2002**, *18*, 3880−3885.
(28) Fields-Zinna, C.; Crowe, M. C.; Dass, A.; Weaver, J. E. F.; Murray, R. W. Mass Spectrometry of Small Bimetal Monolayer-Protected Clusters. *Langmuir* **2009**, *25*, 7704−7710.
(29) Ferrando, R.; Fortunelli, A.; Johnston, R. L. Searching for the Optimum Structures of Alloy Nanoclusters. *Phys. Chem. Chem. Phys.* **2008**, *10*, 640−649.
(30) Yang, H.; Wang, Y.; Huang, H.; Gell, L.; Lehtovaara, L.; Malola, S.; Hakkinen, H.; Zheng, N. All-Thiol-Stabilized Ag_{44} and $Au_{12}Ag_{32}$ Nanoparticles with Single-Crystal Structures. *Nat. Commun.* **2013**, *4*, 2422.
(31) Negreiros, F. R.; Kuntová, Z.; Barcaro, G.; Rossi, G.; Ferrando, R.; Fortunelli, A. Structures of Gas-Phase Ag−Pd Nanoclusters: A Computational Study. *J. Chem. Phys.* **2010**, *132*, 234703.
(32) Guzman, J.; Gates, B. Catalysis by Supported Gold: Correlation between Catalytic Activity for CO Oxidation and Oxidation States of Gold. *J. Am. Chem. Soc.* **2004**, *126*, 2672−2673.
(33) Li, H.; Li, L.; Pedersen, A.; Gao, Y. Magic-Number Gold Nanoclusters with Diameters from 1 to 3.5 Nm: Relative Stability and Catalytic Activity for CO Oxidation. *Nano Lett.* **2014**, *15*, 682−688.
(34) Burch, R. Gold Catalysts for Pure Hydrogen Production in the Water-Gas Shift Reaction: Activity, Structure and Reaction Mechanism. *Phys. Chem. Chem. Phys.* **2006**, *8*, 5483−5500.
(35) Pasquato, L.; Rancan, F.; Scrimin, P.; Mancin, F.; Frigeri, C. *N*-Methylimidazole-Functionalized Gold Nanoparticles as Catalysts for Cleavage of a Carboxylic Acid Ester. *Chem. Commun.* **2000**, *2*, 2253−2254.
(36) Wang, A.; Chang, C.; Mou, C. Evolution of Catalytic Activity of Au−Ag Bimetallic Nanoparticles on Mesoporous Support for CO Oxidation. *J. Phys. Chem. B* **2005**, *109*, 18860−18867.
(37) Chaki, N.; Tsunoyama, H. Effect of Ag-Doping on the Catalytic Activity of Polymer-Stabilized Au Clusters in Aerobic Oxidation of Alcohol. *J. Chem. Phys. C* **2007**, *111*, 4885−4888.
(38) Dass, A. Faradaurate Nanomolecules: A Superstable Plasmonic 76.3 kDa Cluster. *J. Am. Chem. Soc.* **2011**, *133*, 19259−19261.
(39) Kumara, C.; Dass, A. $Au_{329}(SR)_{84}$ Nanomolecules: Compositional Assignment of the 76.3 kDa Plasmonic Faradaurates. *Anal. Chem.* **2014**, *86*, 4227−4232.
(40) von Issendorff, B.; Palmer, R. E. A New High Transmission Infinite Range Mass Selector for Cluster and Nanoparticle Beams. *Rev. Sci. Instrum.* **1999**, *70*, 4497−4501.
(41) Pratontep, S.; Preece, P.; Xirouchaki, C.; Palmer, R. E.; Sanz-Navarro, C. F.; Kenny, S. D.; Smith, R. Scaling Relations for Implantation of Size-Selected Au, Ag, and Si Clusters into Graphite. *Phys. Rev. Lett.* **2003**, *90*, 055503.
(42) Pratontep, S.; Carroll, S. J.; Xirouchaki, C.; Streun, M.; Palmer, R. E. Size-Selected Cluster Beam Source Based on Radio Frequency Magnetron Plasma Sputtering and Gas Condensation. *Rev. Sci. Instrum.* **2005**, *76*, 045103.
(43) Koch, C. D. Determination of Core Structure Periodicity and Point Defect Density along with Dislocation. *Ph.D. Thesis*, Arizona State University, Arizona, 2002.
(44) Young, N. P.; Li, Z. Y.; Chen, Y.; Palomba, S.; Di Vece, M.; Palmer, R. E. Weighing Supported Nanoparticles: Size-Selected Clusters as Mass Standards in Nanometrology. *Phys. Rev. Lett.* **2008**, *101*, 246103.
(45) Wang, Z. W.; Toikkanen, O.; Yin, F.; Li, Z. Y.; Quinn, B. M.; Palmer, R. E. Counting the Atoms in Supported, Monolayer-Protected Gold Clusters. *J. Am. Chem. Soc.* **2010**, *132*, 2854−2855.
(46) Jian, N.; Stapelfeldt, C.; Hu, K.; Fröba, M.; Palmer, R. E. Hybrid Atomic Structure of the Schmid Cluster $Au_{55}(PPh_3)_{12}Cl_6$ Resolved by Aberration-Corrected STEM. *Nanoscale* **2014**, *7*, 885−888.
(47) Wang, Z. W.; Li, Z. Y.; Park, S. J.; Abdela, a.; Tang, D.; Palmer, R. E. Quantitative Z-Contrast Imaging in the Scanning Transmission Electron Microscope with Size-Selected Clusters. *Phys. Rev. B: Condens. Matter Mater. Phys.* **2011**, *84*, 073408.
(48) Wang, Z. W.; Palmer, R. E. Intensity Calibration and Atomic Imaging of Size-Selected Au and Pd Clusters in Aberration-Corrected HAADF-STEM. *J. Phys. Conf. Ser.* **2012**, *371*, 012010.

DOI: 10.1021/jp5119103
J. Phys. Chem. C 2015, 119, 11114−11119

(49) Wang, Z. W.; Toikkanen, O.; Quinn, B. M.; Palmer, R. E. Real-Space Observation of Prolate Monolayer-Protected Au(38) Clusters Using Aberration-Corrected Scanning Transmission Electron Microscopy. *Small* **2011**, *7*, 1542−1545.
(50) Wang, Z. W.; Palmer, R. E. Determination of the Ground-State Atomic Structures of Size-Selected Au Nanoclusters by Electron-Beam-Induced Transformation. *Phys. Rev. Lett.* **2012**, *108*, 245502.
(51) Wang, Z. W.; Palmer, R. E. Experimental Evidence for Fluctuating, Chiral-Type Au_{55} Clusters by Direct Atomic Imaging. *Nano Lett.* **2012**, *12*, 5510−5514.
(52) Plant, S. R.; Cao, L.; Yin, F.; Wang, Z. W.; Palmer, R. E. Size-Dependent Propagation of Au Nanoclusters through Few-Layer Graphene. *Nanoscale* **2014**, *6*, 1258−1263.
(53) Ascencio, J.; Pérez, M.; José-Yacamán, M. A Truncated Icosahedral Structure Observed in Gold Nanoparticles. *Surf. Sci.* **2000**, *447*, 73−80.
(54) Häkkinen, H. Atomic and Electronic Structure of Gold Clusters: Understanding Flakes, Cages and Superatoms from Simple Concepts. *Chem. Soc. Rev.* **2008**, *37*, 1847−1859.
(55) Yang, H.; Wang, Y.; Huang, H.; Gell, L.; Lehtovaara, L.; Malola, S.; Hakkinen, H.; Zheng, N. All-Thiol-Stabilized Ag_{44} and $Au_{12}Ag_{32}$ Nanoparticles with Single-Crystal Structures. *Nat. Commun.* **2013**, *4*, 2422.
(56) Malola, S.; Lehtovaara, L.; Knoppe, S.; Hu, K. J.; Palmer, R. E.; Bürgi, T.; Häkkinen, H. $Au_{40}(SR)_{24}$ Cluster as a Chiral Dimer of 8-Electron Superatoms: Structure and Optical Properties. *J. Am. Chem. Soc.* **2012**, *134*, 19560−19563.
(57) Baletto, F.; Ferrando, R.; Fortunelli, a.; Montalenti, F.; Mottet, C. Crossover among Structural Motifs in Transition and Noble-Metal Clusters. *J. Chem. Phys.* **2002**, *116*, 3856−3863.
(58) Wang, B.; Liu, M.; Wang, Y.; Chen, X. Structures and Energetics of Silver and Gold Nanoparticles. *J. Phys. Chem. C* **2011**, *155*, 11374−11381.
(59) Barnard, A. S.; Young, N. P.; Kirkland, A. I.; Van Huis, M. a.; Xu, H. Nanogold: A Quantitative Phase Map. *ACS Nano* **2009**, *3*, 1431−1436.
(60) Benten, W.; Nilius, N.; Ernst, N.; Freund, H. J. Photon Emission Spectroscopy of Single Oxide-Supported Ag-Au Alloy Clusters. *Phys. Rev. B: Condens. Matter Mater. Phys.* **2005**, *72*, 045403.

DOI: 10.1021/jp5119103
J. Phys. Chem. C 2015, 119, 11114−11119